Supplementary Information (SI) for Journal of Materials Chemistry A.

Supporting Information

Molecular Locking of Defects via H-Bonding/Coordination Dual-Interaction Enables Efficient Perovskite Solar Cells

Yansen Guo,‡[ab] Hailong Huang,‡[a] Yiqing Zhang,‡[c] Zewu Feng, [a] Yanbo Wang, [a] Jianjun Xu, [a] Huanyu Zhang, [a] Yi Ji, [a] Le Li, [a] Chenghao Ge, [a] Xueqi Wu, [a] Yitong Liu, [a] Xin Li, [a] Yige Peng, [a] Chaopeng Huang, [b] Yurou Zhang, [b] Jingsong Sun, [b] Siyu Chen, [d] Weichang Zhou, [d] Dongsheng Tang, [d] Jefferson Zhe Liu, [e] Klaus Weber, [c] Youyong Li, [a] Bin Ding,[f] Hualin Zhan,[c] Xiaohong Zhang, [a] Jun Peng*[ab]*

[a] *Institute of Functional Nano and Soft Materials (FUNSOM), Jiangsu Key Laboratory of Advanced Negative Carbon Technologies, Soochow University, Suzhou 215123, China*

[b] *Zhejiang Baima Lake Laboratory Co., Ltd., Hangzhou Zhejiang 310000, China*

[c] *School of Engineering, The Australia National University, Acton, ACT 2601, Australia*

[d] *School of Physics and Electronics, Key Laboratory of Low-dimensional Quantum Structures and Quantum Control of Ministry of Education, Key Laboratory for Multifunctional Ionic Electronic Materials and Devices of Hunan Normal University, Hunan Province Fundamental Research Center for Quantum Effects and Quantum Technology, Hunan Normal University, Changsha 410081, P. R. China*

[e] *Department of Mechanical Engineering, The University of Melbourne, Parkville, VIC 3010, Australia*

[f] *College of Chemistry, Chemical Engineering and Materials Science, Soochow University, Suzhou 215123, China.*

Corresponding Author

* Hualin Zhan E-mail: hualin.zhan@anu.edu.au

* Jun Peng E-mail: jpeng@suda.edu.cn

Experimental Section

Materials.

Lead iodide (PbI_2, 99.99%), [4-(3,6-Dimethyl-9*H*-carbazol-9-yl)butyl] phosphonic Acid (Me-4PACz, >99%) were purchased from Tokyo Chemical Industry Co., Ltd (TCI). Lead bromide ($PbBr_2$, 99.5%), methylammonium iodide (MAI, 99.9%), methylammonium bromide (MABr, 99.5%), formamidinium iodide (FAI, 99.9%), and methylammonium chloride (MACl, 99.9%) were purchased from Xi'an Yuri Solar Co., Ltd. Sublimed fullerene (C_{60}, 99.95%) was purchased from Advanced Election Technology CO,. Ltd. N,N-dimethylformamide (DMF, 99.8%), dimethyl sulfoxide (DMSO, 99.9%), chlorobenzene (CB, 99.8%), isopropanol (IPA, 99.8%), cesium chloride (CsCl, 99.9%), ethyl alcohol (ETOH, anhydrous, ≥99.9%) were purchased from Sigma-Aldrich. 4-methylsulfonylbenzoic acid (4-MeSBA, >99.5%) was purchased from Admas. Fluorine-doped tin oxide (FTO) substrates were custom-made by Suzhou ShangYang Solar Technology. Tetrakis(dimethylamino)tin(IV) (TDMASn, 99.9999%) was purchased from Shanghai Yuanxiang Chemical Co., Ltd. Additionally, piperazinium iodide (PI, 99.8%) was supplied by Shanghai Aladdin Biochemical Technology Co., Ltd. The ITO target (purity >99.9%) used for sputtering was purchased from Zhongnuo Advanced Material (Beijing) Technology Co., Ltd. All the chemicals were used as received without further purification.

Perovskite Precursor Solution Preparation.

A 1.4 M perovskite precursor solution was prepared by dissolving $Cs_{0.05}MA_{0.05}FA_{0.9}PbI_3$ powder in a mixed solvent of DMF and DMSO (volume ratio 4:1), with a total volume of 1 mL. To promote crystallization, an additional 20% of MACl and 5% of PbI_2 were added to the solution. Different concentrations (0.5, 1.0, and 2.0 mg/mL) of perovskite precursor solutions were prepared by adding 4-MeSBA. For the target perovskite, 1 mg of 4-MeSBA was incorporated into the precursor solution.

Device Fabrication.

Transparent conductive oxide glass substrates, FTO glass, were used as transparent electrodes. The glass substrates were sequentially immersed in detergent, deionized water, acetone, and isopropanol, with each solution being sonicated for 20 minutes. Prior to use, the substrates were blown dry with nitrogen and treated with UV-ozone for 20 minutes. Me-4PACz (SAMs) at a concentration of 1 mg/mL, was spin-coated onto the cleaned FTO substrates. The spin-coating process was carried out at 3000 rpm for 30 seconds, followed by a thermal annealing process at 100°C for 10 minutes. For the perovskite layer preparation, 80 μL of the perovskite precursor solution was spin-coated onto the SAMs substrate. The spin-coating process involved a two-step procedure: 2000 rpm for 10 seconds, followed by 4000 rpm for 30 seconds. Notably, 150 μL of chlorobenzene as the anti-solvent was dropped during the last 10 seconds of the spin-coating process. After spin-coating, the films were annealed at 100°C for 60 minutes, followed by an additional annealing at 150°C for 10 minutes. For the surface passivation layer, PI (0.3 mg/mL in IPA) was dynamically spin-coated onto the perovskite layer.[1,2] The optimized spin-coating parameters were 5000 rpm for 30 seconds and annealed for 10 minutes. For the electron transport layer (ETL), 25 nm of C_{60} was thermally deposited under low vacuum conditions (1×10^{-5} Pa). Following the C60 deposition, the substrates were moved to an atomic layer deposition (ALD) system, and a 20 nm film of SnO_X was deposited at 80°C using tetrakis(dimethylamino) tin (IV) (99.9999% purity) along with deionized water as precursors. Finally, the 200 nm Ag electrode was evaporated by thermal evaporation. For the stability test, a 50 nm-thick ITO layer was deposited between the ALD-SnO_X and Ag electrode by radiofrequency magnetron sputtering at 120 W and 20 sccm Ar gas using an ITO target under a pressure of 2 pa. Note that an anti-reflection film was applied to the glass side of the FTO substrate for all cell devices. The encapsulation method of the PSCs were processed according to previous report.[3]

Characterization of Devices Performance.

Current density-voltage (*J-V*) characterization was performed under an AM 1.5G solar light spectrum using a Newport solar simulator (Class AAA, 94023A-U) and a Keithley 2400 digital source meter. The light intensity was calibrated using a KG-5 standard silicon cell, consistent with the National Photovoltaic Calibration Center. The *J-V* curves were obtained by reverse scanning (1.2 V to 0 V) and forward scanning (0 V to 1.2 V). The effective area of the solar cell was defined by a metal mask with an area of 0.06 cm^2. All *J-V* tests were conducted in ambient conditions. Additionally, external quantum efficiency (EQE) measurements were conducted under ambient conditions using equipment from Enli Tech (QE-R3011) coupled with an Oriel Cornerstone 130 monochromator and optical filters. The steady-state maximum power conversion efficiency was collected by tracking the maximum power point under continuous illumination with a light intensity of 100 mW cm^{-2} (AM1.5G) for 300 seconds in ambient conditions. For operational stability test, encapsulated devices were stored in an ambient condition under continuous illumination.

Other Characterizations

X-ray Photoelectron Spectroscopy (XPS) was obtained using a Kratos AXIS Ultra DLD ultrahigh vacuum photoemission spectroscopy system and Ultraviolet Photoelectron Spectroscopy (UPS) were performed using the Omicron Nanotechnology system. The XPS peak positions of various elements were calibrated by referencing the binding energy of the C 1s peak at 284.8 eV. UPS measurements were conducted using an additional He plasma lamp with an irradiation energy of 21.22 eV. Field Emission Scanning Electron Microscopy (FESEM) images were obtained using a Hitachi SU8230 microscope under 10kV accelerating voltage. Atomic Force Microscopy (Cypher S AFM, Asylum Research, Oxford Instruments) and Kelvin Probe Force Microscopy (KPFM) were used to characterize surface properties. Ultraviolet-visible absorption spectra (UV-vis) were obtained using a PE750 UV-VIS-NIR Spectrophotometer (PerkinElmer model Lambda 750). Fourier-transform infrared (FTIR) spectra were collected using a Fourier Transform Micro-Infrared Spectrometer V70. Nuclear Magnetic Resonance (NMR) spectroscopy was performed using a Bruck Avance III 400 MHz NMR spectrometer, with conditions set at a magnetic field strength of 400 MHz, using deuterated DMSO (DMSO-d6) as the solvent. X-ray Diffraction (XRD) data were acquired with an X-ray diffractometer (PANalytical XRD). Steady-state Photoluminescence (PL) and Time-Resolved Photoluminescence (TRPL) measurements were performed using a Fluorescence Spectrometer (HORIBA Jobin-Yvon LabRAM HR800), equipped with a time-correlated single-photon counting (TCSPC) system and an excitation laser at 485 nm. Additionally, Photoluminescence Mapping (PL mapping) was conducted using a Confocal Raman Imaging System (Alpha 300R). Electrochemical Impedance Spectroscopy (EIS), Transient Photovoltage (TPV), Mott-Schottky was carried out using a Zahner IM6 Electrochemical Workstation. Nyquist curve tests were conducted in the dark, with parameters set at the open-circuit voltage and frequency ranging from 1 MHz to 100 Hz. Mott-Schottky curves were obtained by testing different devices at a specific frequency of 50 kHz. Open-circuit voltage with light intensity curves were collected using filters of different wavelength ranges.

Density functional theory (DFT) calculation.

Gaussian 16 was implemented for the geometry optimization and electrostatic potential (ESP) calculation of molecules. The geometry optimization applied B3LYP functional with 6-3(d,p) basis set, and disperse correction of GD3BJ, the same configuration is applied for latter ESP and molecule energy calculations. Pictures related to Gaussian calculation were drawn by gaussview 6.

VASP 6.3.0 was used for calculation related to perovskite absorb slab model. Slab model used $FAPbI_3$ Crystal with lattice parameter of a=b=c=6.3613Å, α=β=γ=90° to build a 3×3×2 supercell with vacuum layer thickness of 15 Å for molecule absorption simulation. In geometry optimization aspect, the exchange-correlation interaction were treated with the generalized gradient approximation(PAW) of Perdew-Burke-Ernzerhof (PBE) parametrization, with Van-der-waals correction in D3 method to release the energy underestimate problem,[4] this procedure selected to use a k-space of 2×2×1 Monkhorst-Pack with the plane-wave energy cut-off in 400 eV, and only layer near the vacuum layer was allowed to be relaxed. All geometry optimizations finished till energy tolerance reached to 10^{-5} eV/Å and force tolerance reached to 0.02 eV/Å. PBE and D3 correlation described for geometry optimization part were also applied in further energy and charge density calculation, both used a k-space of 4×4×2 Monkhorst-Pack with the plane-wave energy cut-off in 530 eV. The energy tolerance reached 10^{-5} eV/ Å in energy and charge density calculation. All pictures related to slab model were drawn by VESTA.[5]

Formula followed was used for binding energy calculation:

$$E_B = E_T - E_{Perovskite} - E_{Mole}$$

In this formula, E_B is binding energy, E_T is total energy of the slab model that already absorb molecule, $E_{Perovskite}$ is total energy of the perovskite layer without molecule, $E_{Molecule}$ is the total energy of one single molecule in the lattice without perovskite layer.

Formula followed was used for difference charge density calculation, with the assistance of VASPKIT 1.5.1.[6]

$$C_{Diff} = C_{System} - C_{Perovskite} - C_{Molecule}$$

In this formula, C_{Diff} is difference charge density, C_{System} is charge density of while absorption system, $C_{Perovskite}$ is charge density of perovskite surface and $C_{Molecule}$ is charge density of molecule.

Formula followed was used for formation energy calculation:

$$\Delta H_{D,q}(E_F,\mu) = [E_{D,q} - E_H] + \sum_i n_i \mu_i + qE_F$$

In this Formula, $\Delta H_{D,q}(E_F,\mu)$ is the formation energy, $E_{D,q}$ is the total energy of system with defect, E_H is the total energy of system without defect, $\sum_i n_i \mu_i$ is the total chemical potential of defect atoms, n is number of one kind of atom and μ is corresponds chemical potential, qE_F is the total energy of electrons escaped from perovskite bulk, where q is the total charge of electrons, E_F is the fermi level of the whole absorption system.

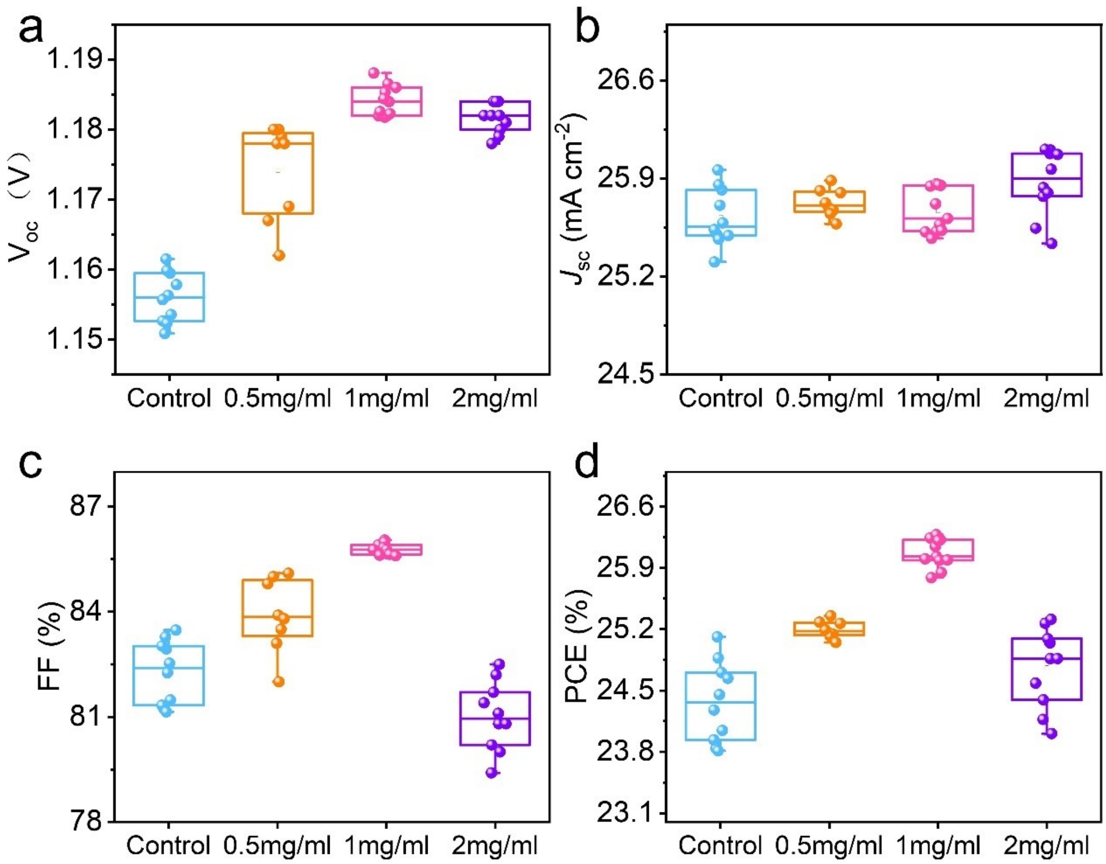

Fig. S1. The photovoltaic performance of devices treated with different concentrations of 4-MeSBA.

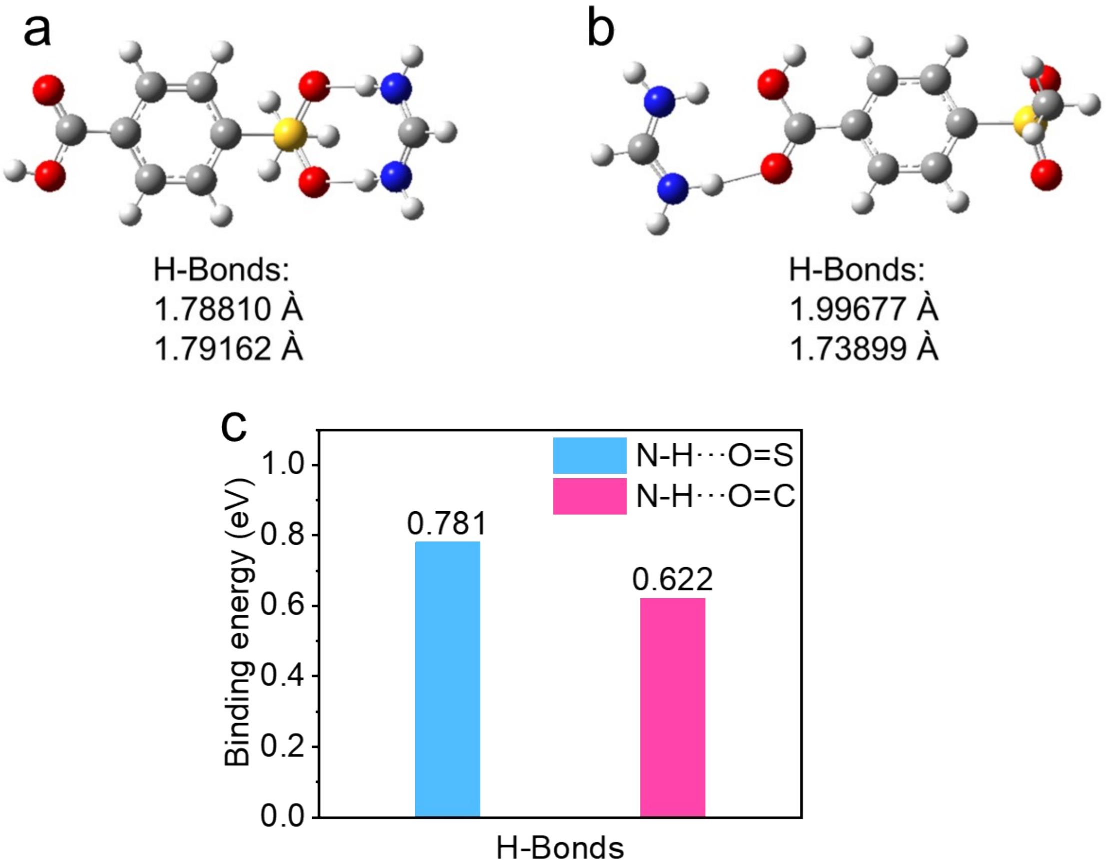

Fig. S2. Hydrogen bonds length and binding energy between FA and the C=O and S=O groups in 4-MeSBA.

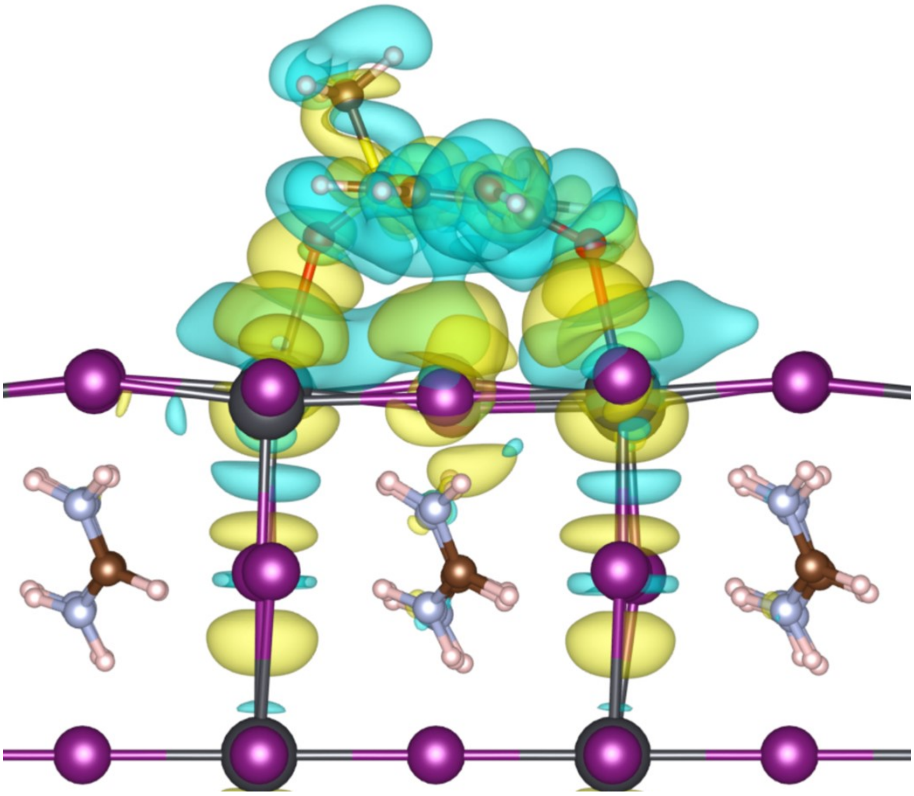

Fig. S3. Differential charge density distribution when 4-MeSBA is adsorbed in a parallel orientation on the perovskite surface.

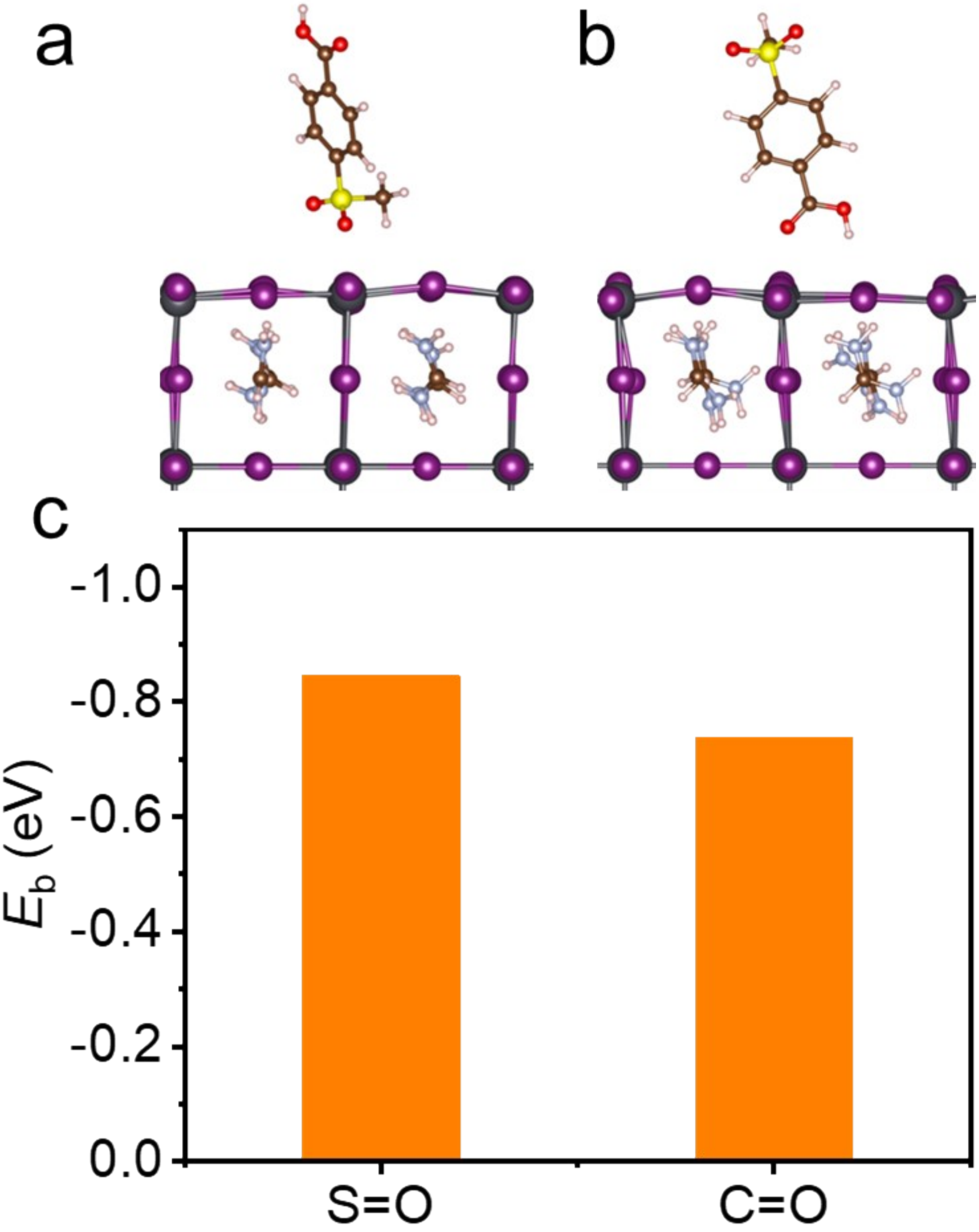

Fig. S4. a, b) Optimized molecular structure of 4-MeSBA and the perovskite lattice model. c) Calculated binding energies between the C=O and S=O groups of 4-MeSBA and Pb^{2+} sites in the perovskite lattice.

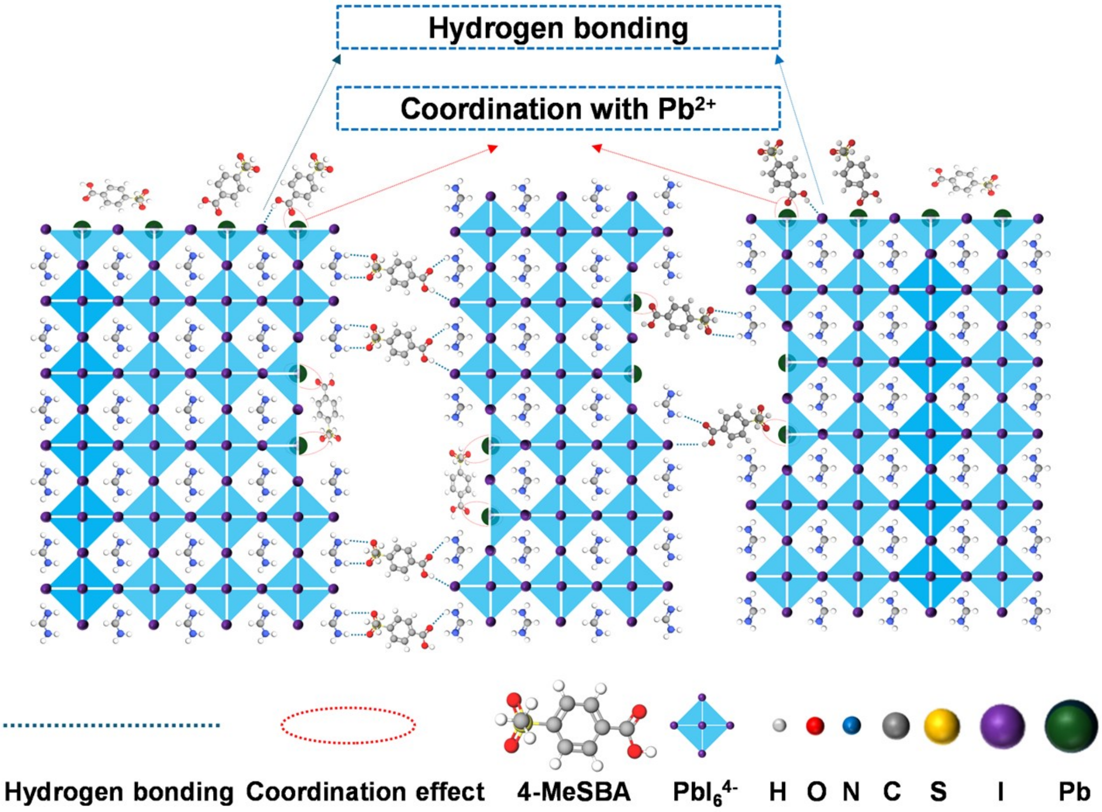

Fig. S5. Illustration of the multifunctional interaction mechanisms of 4-MeSBA in perovskite films.

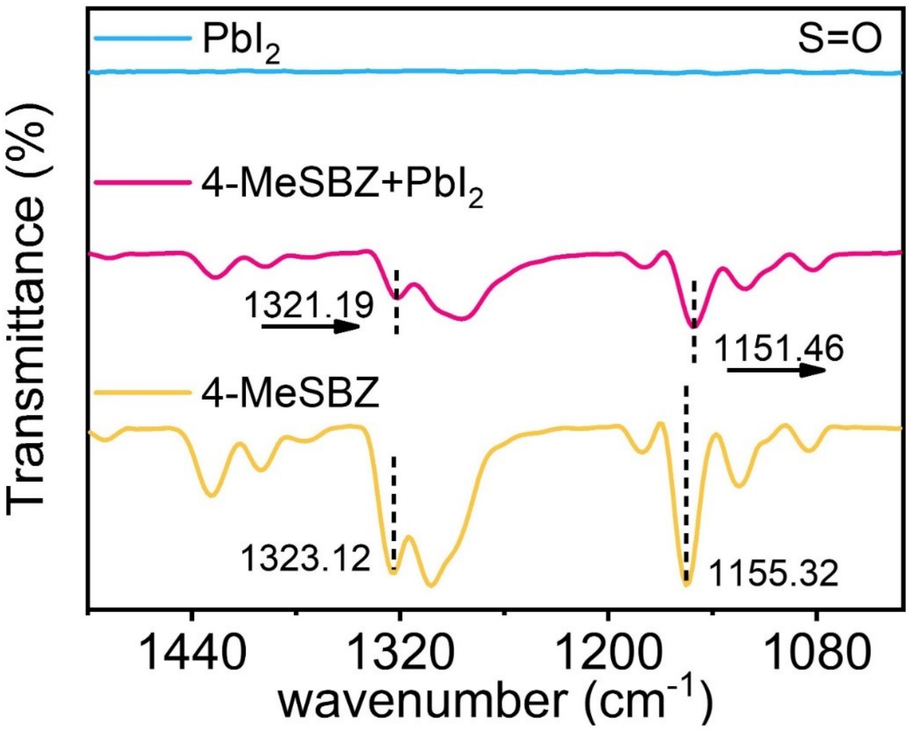

Fig. S6. FTIR spectra focusing on the S=O stretching region for PbI_2, 4-MeSBA, and their mixture, highlighting the interaction between 4-MeSBA and Pb^{2+}.

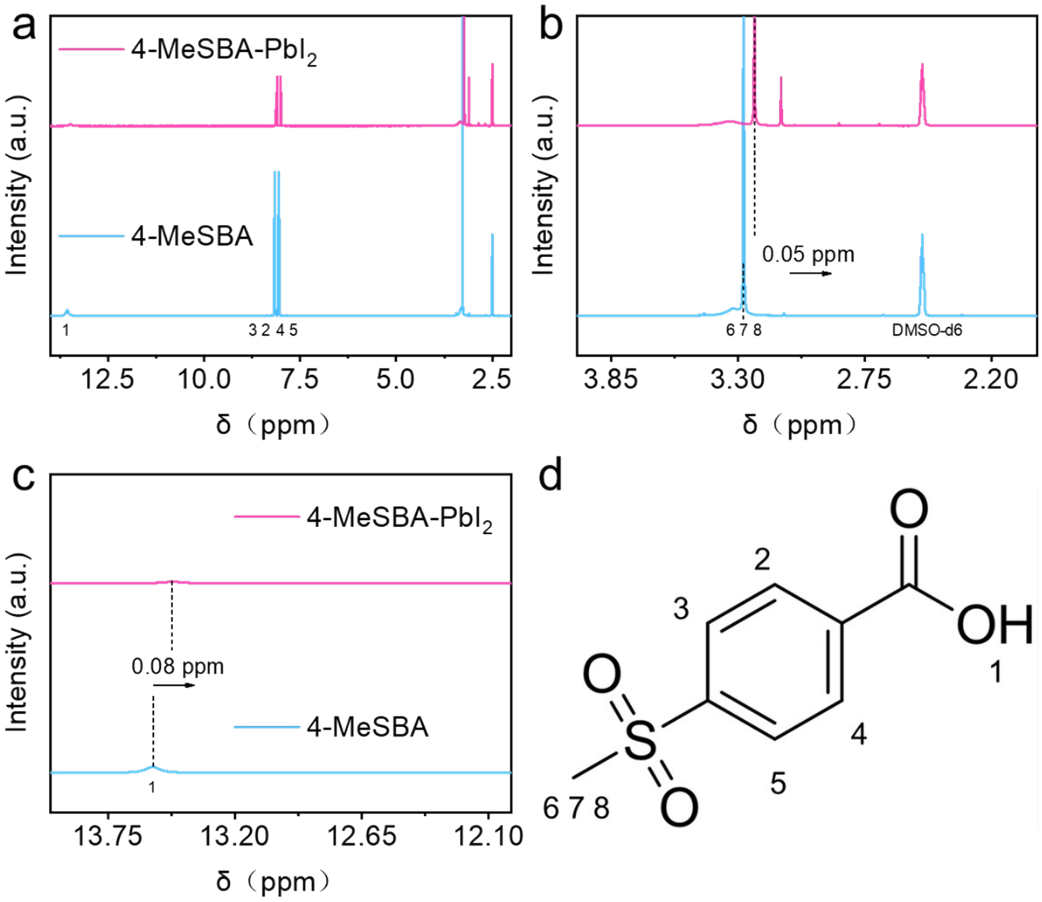

Fig. S7.^{1}H NMR Spectra Before and After Mixing 4-MeSBA with PbI_2. a) Full ^{1}H NMR spectrum. b) High-field shift of methyl protons due to coordination between the S=O bond and Pb^{2+} ions. c) High-field shift of hydroxyl protons due to hydrogen bonding between the carboxyl group and iodide ions. d) Molecular formula of 4-MeSBA.

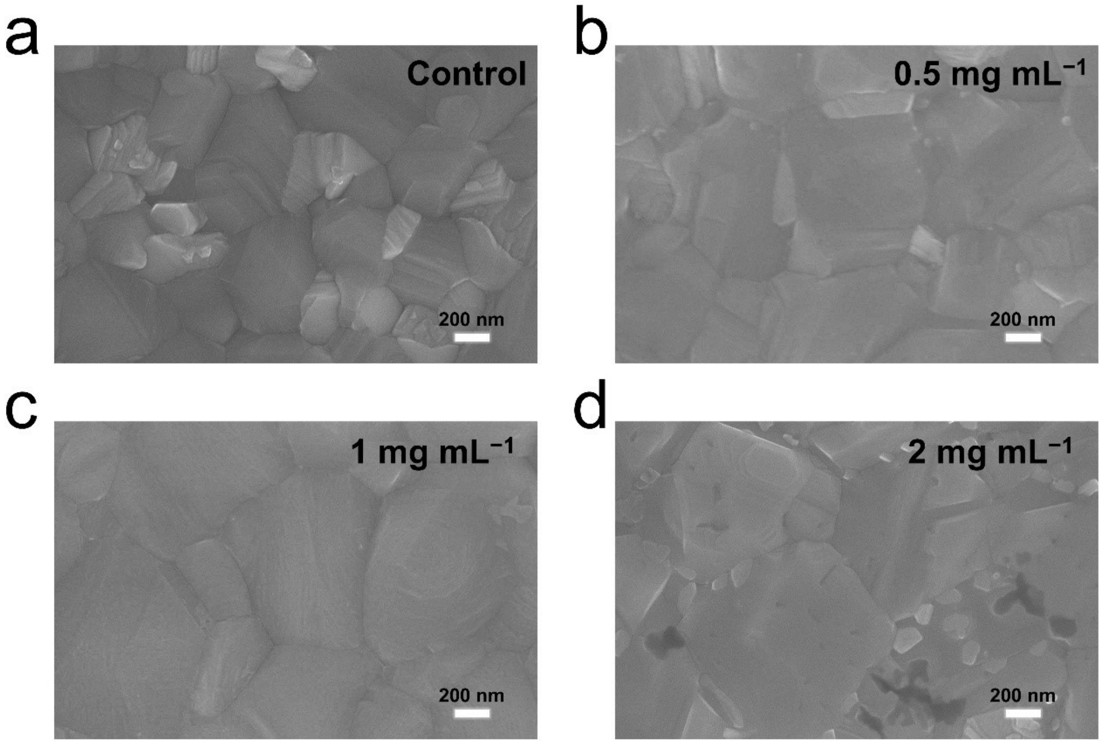

Fig. S8. Top-view SEM images of perovskite films prepared with varying concentrations of 4-MeSBA.

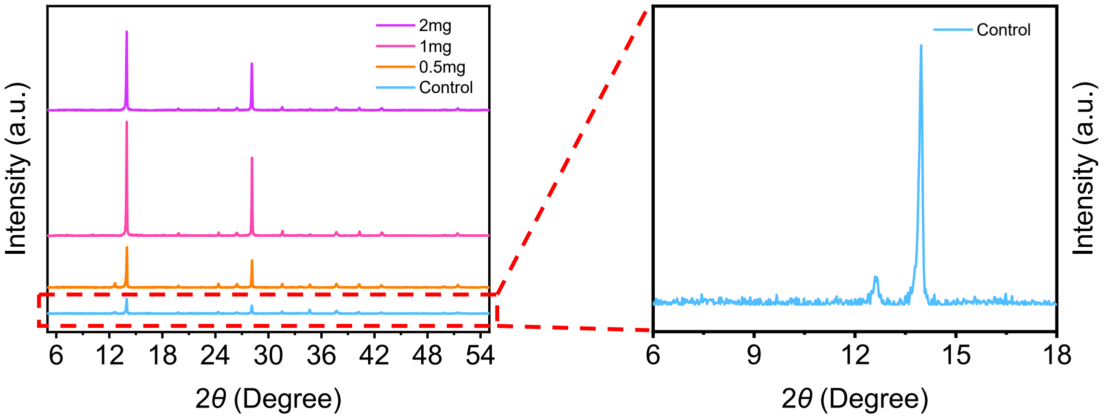

Fig. S9. XRD pattern of perovskite films prepared with varying concentrations of 4-MeSBA.

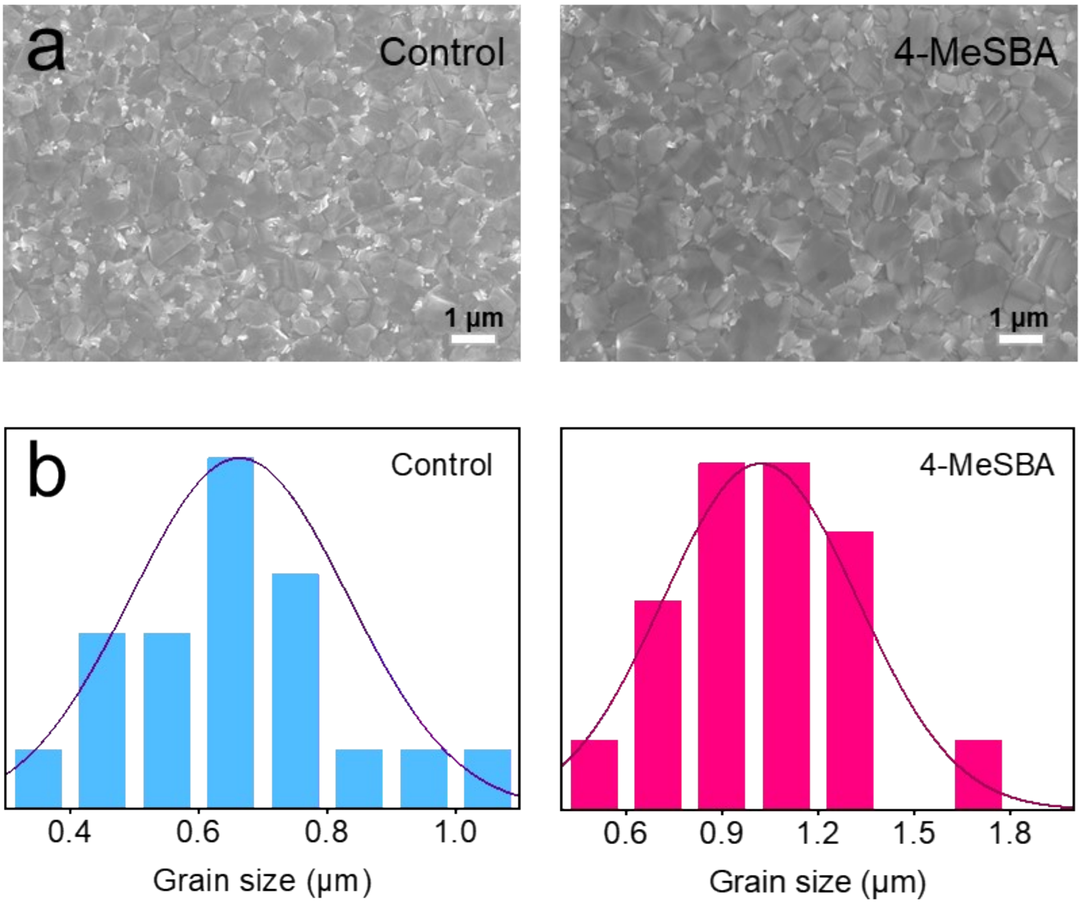

Fig. S10. Scanning Electron Microscopy (SEM) images and Grain Size Distribution of Perovskite Films Before and After 4-MeSBA Treatment.

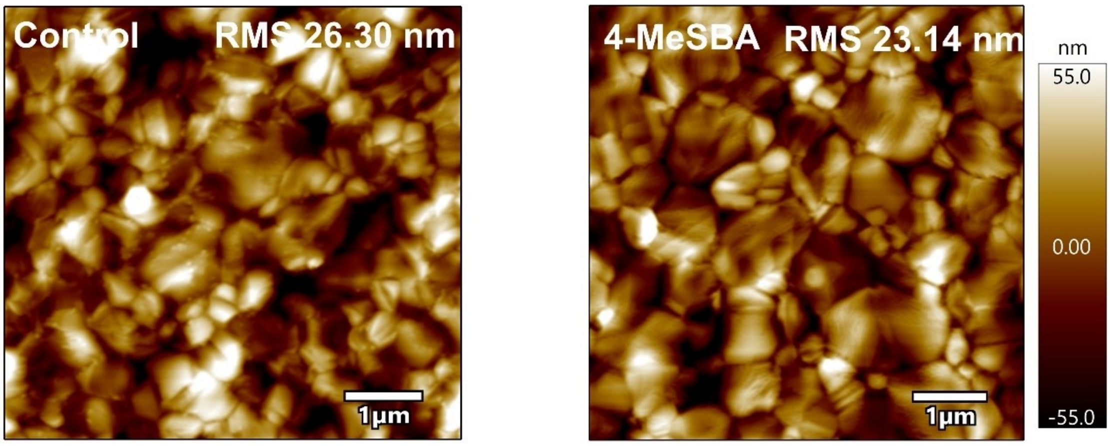

Fig. S11. Atomic Force Microscopy (AFM) results of the films before and after 4-MeSBA treatment.

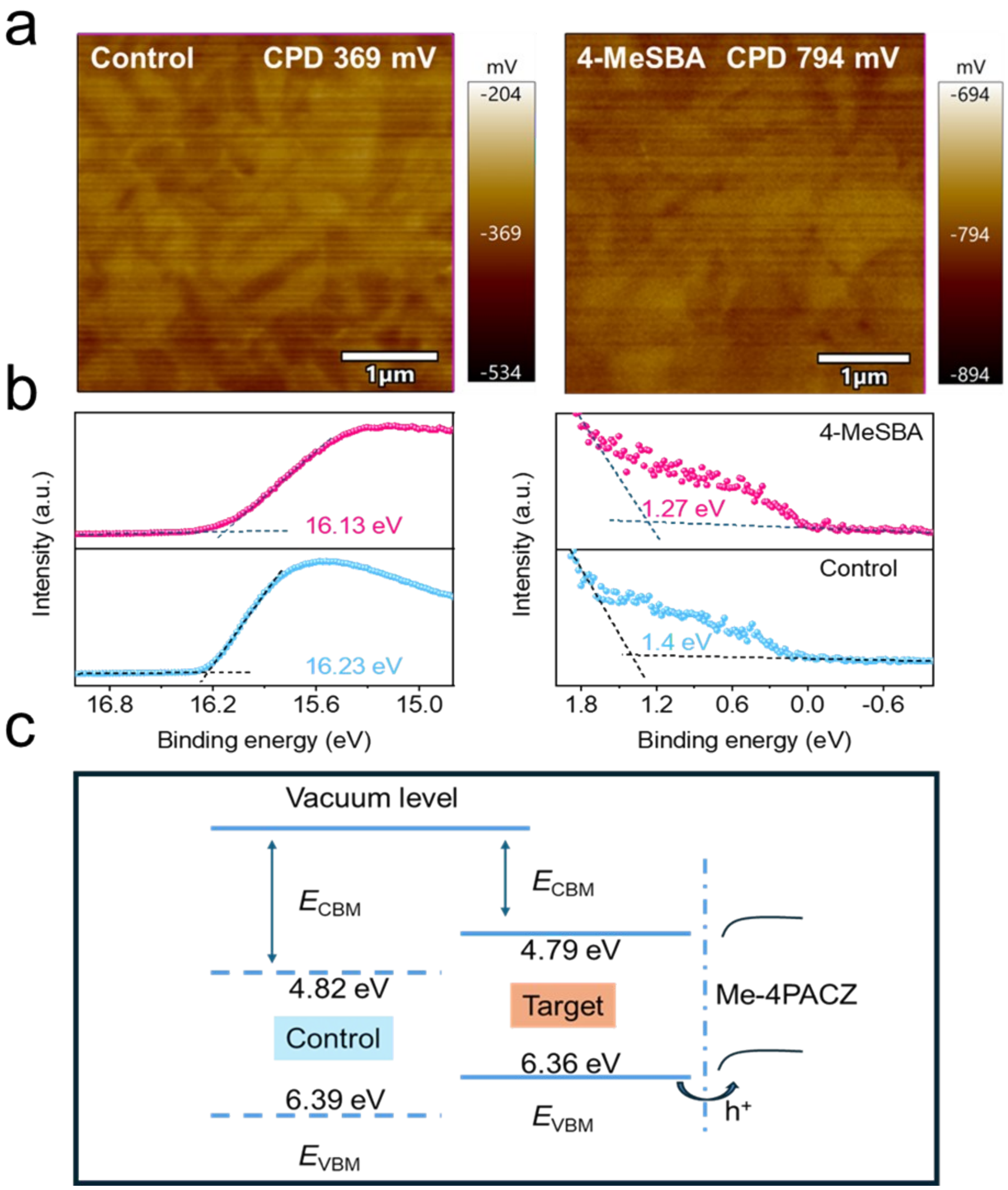

Fig. S12. a) Kelvin probe force microscopy (KPFM) results of the films before and after 4-MeSBA treatment. b, c) Ultraviolet photoelectron spectroscopy (UPS) and energy level image of perovskite films.

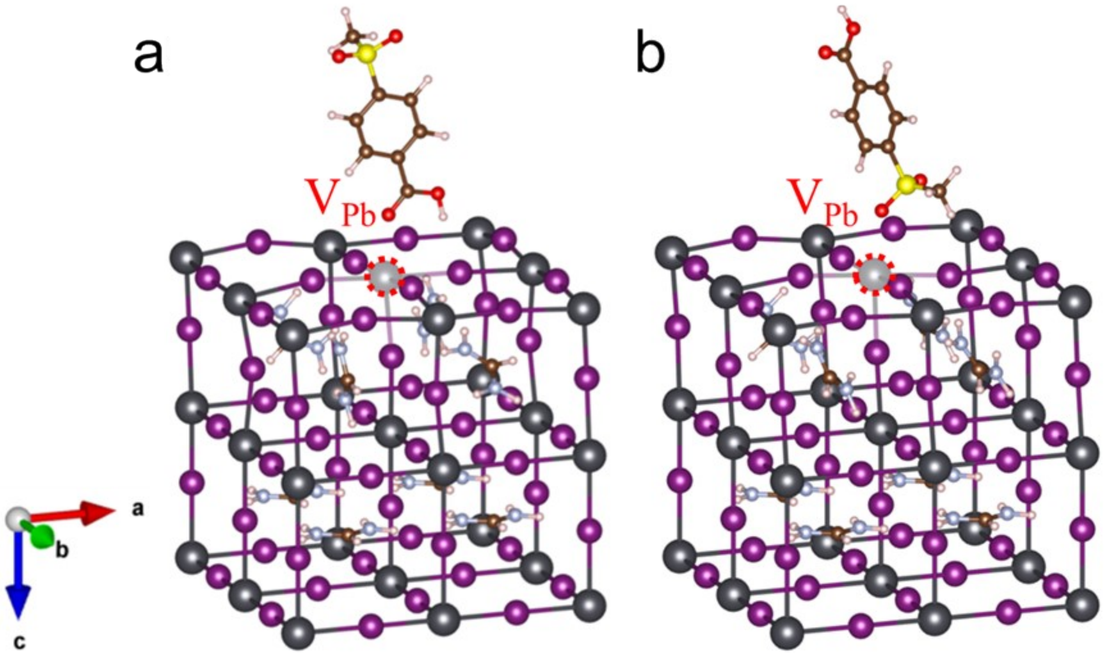

Fig. S13. Atomic structure of Pb vacancies. a) C=O close to the perovskite surface. b) S=O close to the perovskite surface.

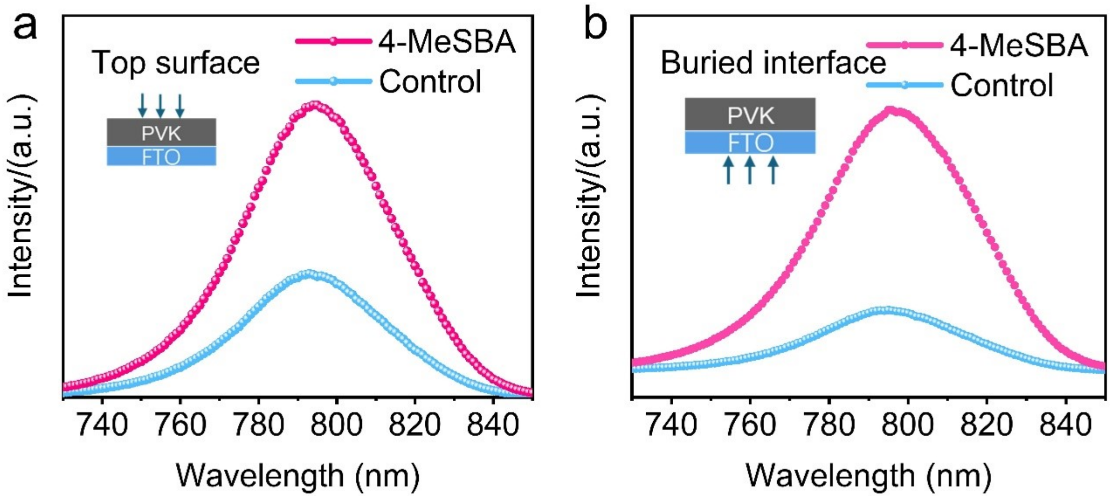

Fig. S14. a) Photoluminescence (PL) spectra obtained from illumination on the surface of control and 4-MeSBA modified perovskite films. b) PL spectra obtained from illumination on the buried interface of control and 4-MeSBA modified perovskite films.

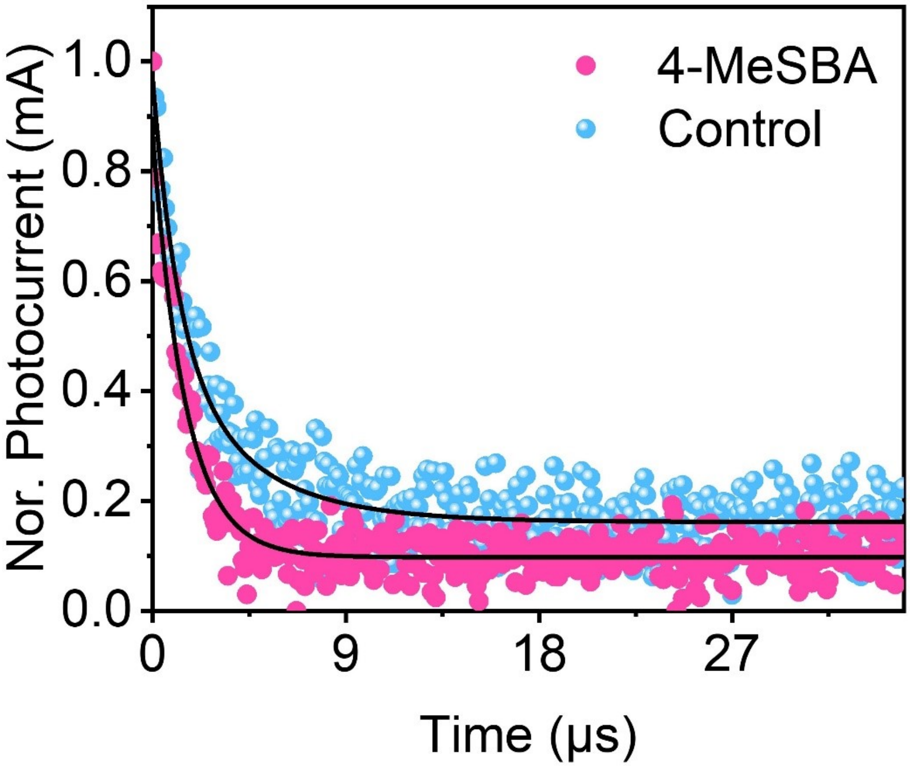

Fig. S15. Transient Photocurrent (TPC) Comparison of Control and 4-MeSBA-Treated Perovskite devices.

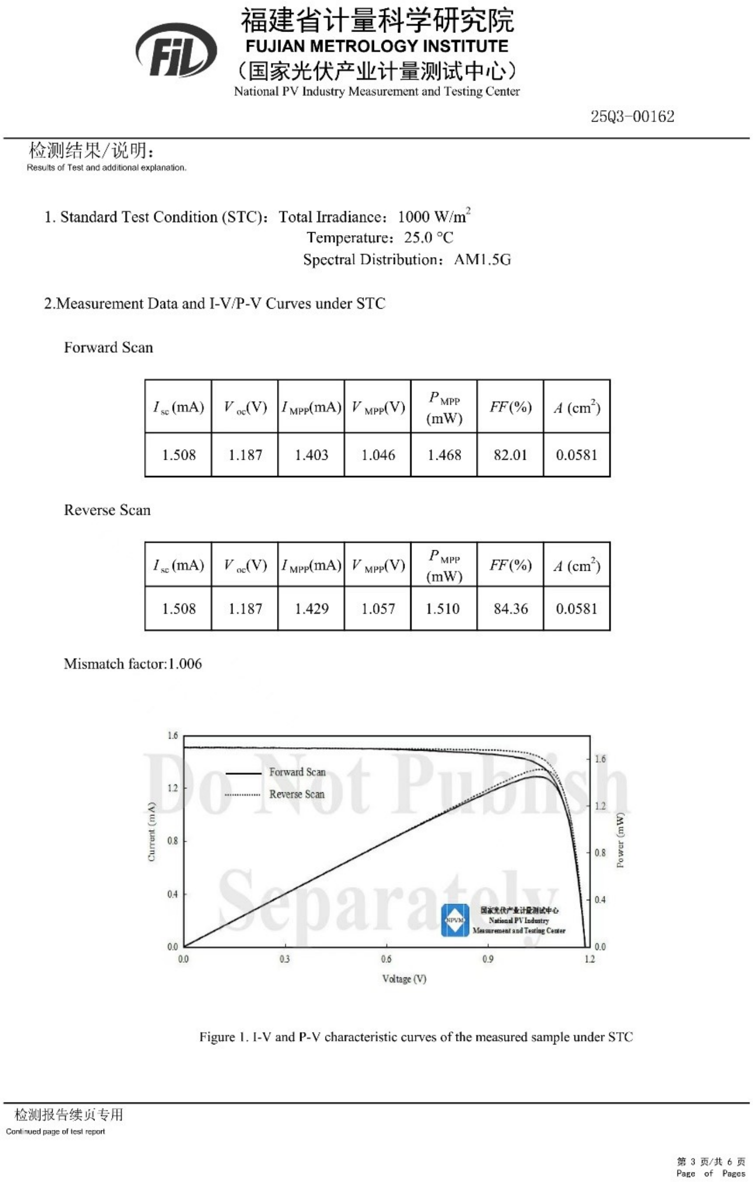

福建省计量科学研究院
FUJIAN METROLOGY INSTITUTE
（国家光伏产业计量测试中心）
National PV Industry Measurement and Testing Center

25Q3-00162

检测结果/说明：
Results of Test and additional explanation.

1. Standard Test Condition (STC)：Total Irradiance：1000 W/m^2
Temperature：25.0 °C
Spectral Distribution：AM1.5G

2.Measurement Data and I-V/P-V Curves under STC

Forward Scan

I_{sc} (mA)	V_{oc}(V)	I_{MPP}(mA)	V_{MPP}(V)	P_{MPP} (mW)	FF(%)	A (cm^2)
1.508	1.187	1.403	1.046	1.468	82.01	0.0581

Reverse Scan

I_{sc} (mA)	V_{oc}(V)	I_{MPP}(mA)	V_{MPP}(V)	P_{MPP} (mW)	FF(%)	A (cm^2)
1.508	1.187	1.429	1.057	1.510	84.36	0.0581

Mismatch factor:1.006

Figure 1. I-V and P-V characteristic curves of the measured sample under STC

检测报告续页专用
Continued page of test report

第 3 页/共 6 页
Page of Pages

Fig. S16. The certification report, including both forward and reverse scan results as well as steady-state efficiency verification, was issued by the NPVM (National PV Industry Measurement and Testing Center).

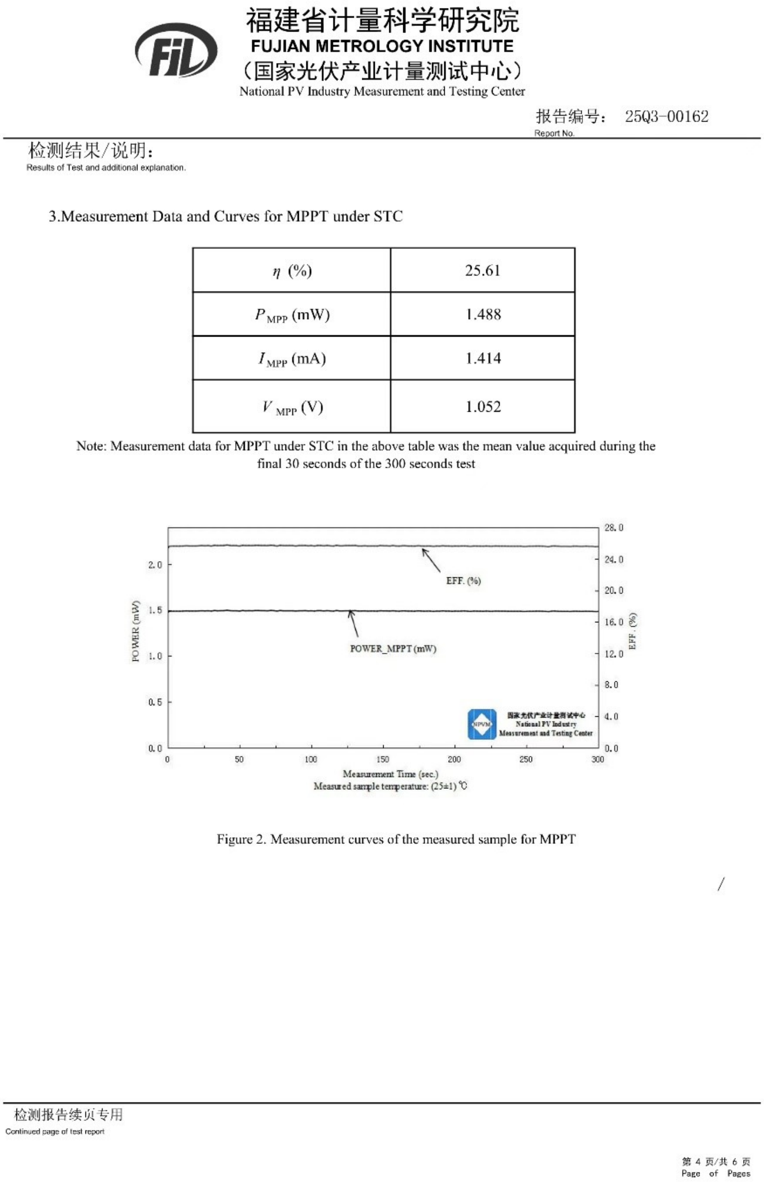

福建省计量科学研究院
FUJIAN METROLOGY INSTITUTE
（国家光伏产业计量测试中心）
National PV Industry Measurement and Testing Center

报告编号： 25Q3-00162
Report No.

检测结果/说明：
Results of Test and additional explanation.

3.Measurement Data and Curves for MPPT under STC

η (%)	25.61
P_{MPP} (mW)	1.488
I_{MPP} (mA)	1.414
V_{MPP} (V)	1.052

Note: Measurement data for MPPT under STC in the above table was the mean value acquired during the final 30 seconds of the 300 seconds test

Figure 2. Measurement curves of the measured sample for MPPT

/

检测报告续页专用
Continued page of test report

第 4 页/共 6 页
Page of Pages

Fig. S16. The certification report, including both forward and reverse scan results as well as steady-state efficiency verification, was issued by the NPVM.

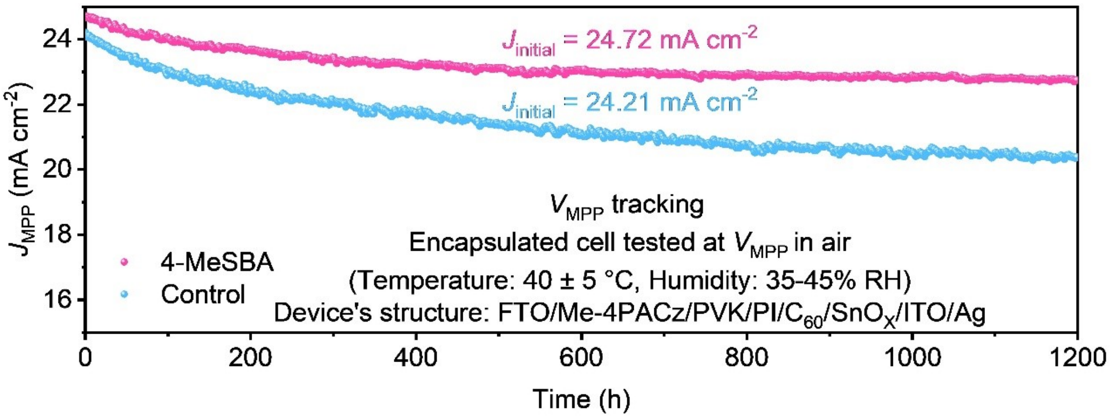

Fig. S17. Long-term stability of current density at the maximum power point (J_{MPP}) under continuous illumination for 1200 hours.

Table S1. Specific Data of TRPL Spectra for Perovskite Films with/without 4-MeSBA additives.

	A_1	τ_1	A_2	τ_2	τ_{ave} (ns)
Control	0.13	76.17	0.72	619.74	607.90
4-MeSBA	0.34	172.93	0.65	3016.35	2934.13

Table S2. Relevant parameters and calculated values of SCLC for Perovskite Devices with/without 4-MeSBA additives.

Sample	Thickness (nm)	V_{TFL} (V)	N_{trap} (cm^{-3})
Control	600	0.570	8.1×10^{15}
4-MeSBA		0.365	5.2×10^{15}

Table S3. Specific Parameters of TPV for Perovskite Devices with/without 4-MeSBA additives.

	A_1	τ_1	A_2	τ_2	τ_{ave} (ns)
Control	0.13	76.17	0.72	619.74	607.90
4-MeSBA	0.34	172.93	0.65	3016.35	2934.13

Table S4. Specific Parameters of TPC for Perovskite Devices with/without 4-MeSBA additives.

	A_1	τ_1	A_2	τ_2	τ_{ave} (μs)
Control	0.47	1.18	0.34	3.86	3.06
4-MeSBA	0.56	1.52	0.21	1.52	1.52

Table S5. Specific Parameters of EIS for Perovskite Devices with/without 4-MeSBA additives.

	R_s (Ohm)	R_{rec} (Ohm)	C_{rec} (F)
Control	5.55	17.93	4×10^{-8}
4-MeSBA	4.79	26.48	6.8×10^{-8}

Table S6. *J-V* Curve Parameters of the Champion Perovskite Devices with/without 4-MeSBA additives.

	V_{OC} (V)	J_{SC} (mA cm^{-2})	FF (%)	PCE (%)
Control	1.163	26.09	83.7	25.40
4-MeSBA	1.188	26.12	84.9	26.35

Table S7. Specific *J-V* curve parameters of the optimal perovskite devices modified with different concentrations of 4-MeSBA.

	V_{OC} (V)	J_{SC} (mA cm^{-2})	FF (%)	PCE (%)	PCE$_{\mathrm{ave}}$ (%)
0 mg/mL	1.160	25.86	82.9	24.87	24.71
0.5 mg/mL	1.162	25.89	82.0	25.35	25.16
1 mg/mL	1.182	25.86	86.0	26.28	26.24
2 mg/mL	1.184	26.11	81.7	25.27	24.59

Table S8. Summary of photovoltaic parameters for devices treated with 4-MeSBA and other representative molecules containing similar functional groups (C=O and/or S=O). Certified power conversion efficiencies are indicated in red for emphasis.

Device Structure	V_{OC} (V)	J_{SC} (mA cm^{-2})	FF (%)	PCE (%)	Reference
NIP	1.24	20.3	81.2	20.47	Angew. Chem. Int. Ed. 2022, 61, e202205012.
PIN	1.21	23.71	81.0	23.18	Adv. Mater. 2023, 35, 2302752.
NIP	1.18	25.37	81.6	24.33	Adv. Energy Mater. 2023, 13, 2300610.
NIP	1.18	25.61	81.2	24.56	Adv. Funct. Mater. 2024, 34, 2314472.
NIP	1.19	24.96	84.6	25.15	Adv. Energy Mater. 2025, 2402856.
NIP	1.18	25.78	84.2	25.71	Angew.Chem. Int.Ed. 2024,

Device Structure	V_{OC} (V)	J_{SC} (mA cm^{-2})	FF (%)	PCE (%)	Reference
				24.66 (Certified)	63, e202410378.
NIP	1.19	26.39	82.9	26.07 25.80 (Certified)	Nature 2023, 623, 531–537.
PIN	1.16	26.14	85.7	26.09 25.81 (Certified)	Nature 2023, 624, 557–563.
PIN	1.15	25.60	82.5	24.31	Energy Environ. Sci., 2024, 17, 9443–9454
PIN	1.20	25.70	84.7	26.10	Angew. Chem. Int. Ed. 2025, e202418883.
PIN	1.19	25.50	84.9	25.84 25.05 (Certified)	Nat Commun 2024, 15, 5607
PIN	1.18	25.79	85.6	26.14	Adv. Funct. Mater. 2025, 2504424.
PIN	1.20	26.30	84.5	26.69 26.54 (Certified)	Nature 2024, 632, 536–542.
PIN	1.17	26.13	85.2	26.90 26.15%	Science 2024, 384, 189.
PIN	**1.19**	**26.12**	**84.9**	**26.35** **26.00 (Certified)**	**This work**

References.

1 S. Liu, J. Li, W. Xiao, R. Chen, Z. Sun, Y. Zhang, X. Lei, S. Hu, M. Kober-Czerny, J. Wang, F. Ren, Q. Zhou, H. Raza, Y. Gao, Y. Ji, S. Li, H. Li, L. Qiu, W. Huang, Y. Zhao, B. Xu, Z. Liu, H. J. Snaith, N.-G. Park and W. Chen, *Nature*, 2024, **632**, 536–542.

2 S. Mariotti, E. Köhnen, F. Scheler, K. Sveinbjörnsson, L. Zimmermann, M. Piot, F. Yang, B. Li, J. Warby, A. Musiienko, D. Menzel, F. Lang, S. Keßler, I. Levine, D. Mantione, A. Al-Ashouri, M. S. Härtel, K. Xu, A. Cruz, J. Kurpiers, P. Wagner, H. Köbler, J. Li, A. Magomedov, D. Mecerreyes, E. Unger, A. Abate, M. Stolterfoht, B. Stannowski, R. Schlatmann, L. Korte and S. Albrecht, *Science*, 2023, **381**, 63–69.

3 R. Lin, Y. Wang, Q. Lu, B. Tang, J. Li, H. Gao, Y. Gao, H. Li, C. Ding, J. Wen, P. Wu, C. Liu, S. Zhao, K. Xiao, Z. Liu, C. Ma, Y. Deng, L. Li, F. Fan and H. Tan, *Nature*, 2023, **620**, 994–1000.

4 S. Grimme, J. Antony, S. Ehrlich and H. Krieg, *J. Chem. Phys.*, 2010, **132**, 154104.

5 K. Momma and F. Izumi, *J. Appl. Crystallogr.*, 2011, **44**, 1272–1276.

6 V. Wang, N. Xu, J.-C. Liu, G. Tang and W.-T. Geng, *Comput. Phys. Commun.*, 2021, **267**, 108033.